Resonantly enhanced superconductivity mediated by spinor condensates

Giacomo Bighin[1], Puneet A. Murthy[2], Nicolò Defenu[3], and Tilman Enss[1]

[1]*Institut für Theoretische Physik, Universität Heidelberg, Heidelberg, Germany*
[2]*Institute for Quantum Electronics, ETH Zürich, Zürich, Switzerland*
[3]*Institute for Theoretical Physics, ETH Zürich, Zürich, Switzerland*
(Dated: December 15, 2022)

Achieving strong interactions in fermionic many-body systems is a major theme of research in condensed matter physics. It is well-known that interactions between fermions can be mediated through a bosonic medium, such as a phonon bath or Bose-Einstein condensate (BEC). Here, we show that such induced attraction can be resonantly enhanced when the bosonic medium is a two-component spinor BEC. The strongest interaction is achieved by tuning the boson-boson scattering to the quantum critical spinodal point of the BEC where the sound velocity vanishes. The fermion pairing gap and the superconducting critical temperature can thus be dramatically enhanced. We propose two experimental realizations of this scenario, with exciton-polariton systems in two-dimensional semiconductors and ultracold atomic Bose-Fermi mixtures.

Fermion pairing is the central ingredient of superconductivity. The Bardeen–Cooper–Schrieffer (BCS) theory [1] provides a paradigmatic model for pairing, where attractive interaction between electrons is mediated by crystal phonons. The strength of such phonon-mediated interactions, however, is typically weak leading to small critical temperatures (T_c) relative to the Fermi temperature (T_F). Enhancing the interaction strength between fermions in order to obtain higher T_c is therefore an important goal in condensed matter physics.

A variety of approaches for inducing and enhancing interactions between fermions have been explored in various systems. In solid state, recent works on twisted bilayer graphene have demonstrated that electronic correlations can be enhanced by careful tuning of the relative angle between graphene layers, which results in flat bands for electrons and consequently high values of $T_c/T_F \sim 0.1$ [2]. In ultracold atomic systems, the use of Feshbach resonances between different hyperfine spin states of atoms allows to reach the strong interaction regime of the BEC-BCS crossover [3]. In the context of boson-mediated interactions, a number of strategies have been proposed to induce interactions using novel bosonic quasiparticles such as exciton-polaritons [4], plasmon-polaritons, and atomic BECs [5–7]. Another recently demonstrated approach consists of illuminating superconductors with short intense pulses of light, which strongly modify the phonon dispersion thereby inducing transient signatures of superconductivity at higher critical temperatures than in equilibrium [8–10].

In this work, we show that coupling a fermionic system to a two-component spinor BEC, i.e., a BEC consisting of two coherently coupled spin components, can have dramatic consequences for the induced interactions between fermions. An illustration of our proposed system is shown in Fig. 1(a), where the orange balls correspond to two species bosons, which interact with a two-component Fermi gas represented by blue balls. To reach strong interactions, we propose to utilize the spinodal instability

of spinor BECs, which can be reached by carefully tuning the inter- and intra-species scattering of the two bosonic components. Coupling fermions to this quantum critical bosonic medium can lead to a resonant enhancement of the induced interactions. We analyse the nature of the induced interactions, and calculate the pairing gap as well as the superconducting temperature of the Fermi system. Finally, we discuss two possible platforms where this effect may be experimentally realized.
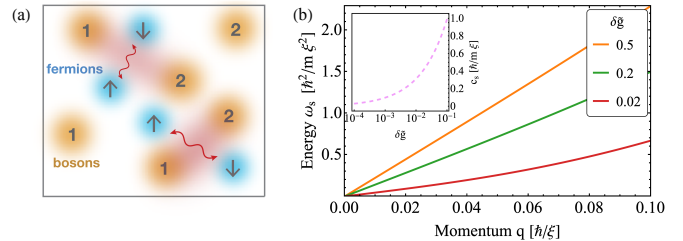
Figure 1. **Fermions in a two-component spinor BEC.** (a) Schematic representation of the induced fermion-fermion pairing mechanism: the normal modes of the spinor BEC mediate the fermion-fermion interaction. By tuning the inter-boson interaction one can make one of the two BEC normal modes arbitrarily soft and resonantly increase the induced fermion-fermion interaction (red line). (b) Dispersion relation for the 'spin' normal mode of the spinor BEC, as a function of the momentum, for three different values of the detuning $\delta\tilde{g} \equiv (m/\hbar^2)\delta g$ from the spinodal point (parameters $\tilde{g}_F = (m/\hbar^2)g_F = 0.2$, $m_1 = m_2 = m$, and $n_1 = n_2$). Inset: speed of sound of the 'spin' normal mode, as a function of $\delta\tilde{g}$; as $\delta\tilde{g} \searrow 0$ the mode becomes arbitrarily soft.

Spinodal instability in two-component BECs. We consider a two-dimensional system consisting of a noninteracting uniform Fermi gas immersed in a spinor BEC, with two spin components labeled 1 and 2. We will first discuss the essential features of the spinor BEC and then move on to the question of coupled Bose-Fermi mixtures. The spinor BEC problem has been extensively studied in previous literature [11–16]. Coupling two BECs

leads to new collective normal modes, which we refer to as density and spin waves. Density waves correspond to in-phase oscillations of the two components, whereas spin waves involve out-of-phase oscillations. Using the Bogoliubov transformation, the bosonic Hamiltonian can be diagonalized and expressed in terms of the density and spin normal modes according to (see Supplement for details) [11, 15, 16]

$$\hat{\mathcal{H}}^{(b)} = \sum_{\mathbf{q}} \omega_{\mathbf{q}}^d \hat{a}_{\mathbf{q}}^\dagger \hat{a}_{\mathbf{q}} + \sum_{\mathbf{q}} \omega_{\mathbf{q}}^s \hat{b}_{\mathbf{q}}^\dagger \hat{b}_{\mathbf{q}}, \qquad (1)$$

where the $\hat{a}_{\mathbf{q}}^\dagger$ ($\hat{b}_{\mathbf{q}}^\dagger$) operators create a density (spin) excitation at momentum $\mathbf{q}$. The Bogoliubov dispersion relation $\omega_{\mathbf{q}}^{d(s)}$ is given at small momenta by

$$\omega_{\mathbf{q}}^{d(s)} \approx \sqrt{\frac{\hbar^2 q^2}{2m}\left(\frac{\hbar^2 q^2}{2m} + 2mc_{d(s)}^2\right)} \qquad (2)$$

for bosons of mass m. The density and spin sound velocities $c_{d(s)}$ depend crucially on the intra- and inter-species interaction strengths between the two bosonic components as

$$c_{d(s)}^2 = \frac{g_{11}n_1 + g_{22}n_2 \pm \sqrt{(g_{11}n_1 - g_{22}n_2)^2 + 4n_1 n_2 g_{12}^2}}{2m}. \qquad (3)$$

Here, g_{11} and g_{22} are the coupling constants between bosons of the same species, while g_{12} is the coupling strength between species 1 and 2. The boson densities of each species are denoted by n_1 and n_2. The $+$ $(-)$ sign corresponds to the density (spin) excitations, respectively.

Careful tuning of the different coupling strengths can lead to dramatic modification of the sound velocities. To see this, we define an effective interaction parameter $\delta g = \sqrt{g_{11}g_{22}} - g_{12}$. For repulsive $g_{12} > 0$ one can tune $\delta g \searrow 0$, and the spin sound velocity to leading order in δg scales as

$$c_s \approx \sqrt{\frac{2g_{12}n_1 n_2}{g_{11}n_1 + g_{22}n_2}}\sqrt{\frac{\delta g}{m}}. \qquad (4)$$

An intriguing consequence of Eq. (4) is that for $\delta g \to 0$, the spin sound velocity vanishes even for finite density and scattering lengths. This point is known as the spinodal instability [16], which marks the transition to the immiscible, phase separated state. [Analogously, for $g_{12} < 0$ the miscible state of the spinor BEC exhibits a transition toward a novel liquid droplet state stabilized by quantum fluctuations [17, 18]; near this transition for $\delta g' = \sqrt{g_{11}g_{22}} + g_{12} \searrow 0$ the spin speed of sound remains finite but instead the density speed of sound becomes soft and vanishes, and with this replacement our conclusions remain unchanged.] In Fig. 1(b), we show the calculated dispersion relation of spin waves for different values of δg, where the softening of the mode at low momenta can be clearly seen as we approach the spinodal point $\delta g \searrow 0$. In the inset of Fig. 1(b), we show the vanishing of the spin sound velocity c_s with decreasing δg.

Induced interactions. Next, we introduce fermions to the system. The single-particle noninteracting Hamiltonian for fermions has the form

$$\hat{\mathcal{H}}^{(f)} = \sum_{\mathbf{k}\sigma} \epsilon_{\mathbf{k}} \hat{c}_{\mathbf{k}\sigma}^\dagger \hat{c}_{\mathbf{k}\sigma}, \qquad (5)$$

where the $\hat{c}_{\mathbf{k}\sigma}^\dagger$ operator creates a fermionic particle of momentum $\mathbf{k}$ and spin $\sigma = \uparrow, \downarrow$. Ultracold Fermi gases can be modeled with a quadratic dispersion relation $\epsilon_{\mathbf{k}} = \hbar^2 k^2 / 2m_F - \mu_F$, where m_F denotes the fermion mass and μ_F is the fermion chemical potential. As the superconducting properties depend predominantly on the density of states $N_0 = m_F/\pi\hbar^2$ near the Fermi surface, our results are robust also for other dispersions $\epsilon_{\mathbf{k}}$ with given N_0. For simplicity and in order to highlight the influence of fermion-boson interactions, we assume that the direct fermion-fermion interactions are negligible; if not, they would be added to our result for the induced interaction.

Let us now consider the interaction between fermions and the spinor BEC, modeled by the contact interaction strengths g_{F1} and g_{F2} between either fermion species and boson components 1 and 2, respectively. When written in terms of the normal modes of the spinor BEC, the interaction term in the Hamiltonian reads

$$\hat{\mathcal{H}}^{(f-b)} = \sum_{\mathbf{k};\mathbf{q}\neq 0} M_d(\mathbf{q})\hat{c}_{\mathbf{k}+\mathbf{q}}^\dagger \hat{c}_{\mathbf{k}}(\hat{a}_{\mathbf{q}} + \hat{a}_{-\mathbf{q}}^\dagger)$$
$$+ \sum_{\mathbf{k};\mathbf{q}\neq 0} M_s(\mathbf{q})\hat{c}_{\mathbf{k}+\mathbf{q}}^\dagger \hat{c}_{\mathbf{k}}(\hat{b}_{\mathbf{q}} + \hat{b}_{-\mathbf{q}}^\dagger). \qquad (6)$$

Here, M_d and M_s are effective interaction vertices between fermions and the density and spin normal modes of the spinor BEC [19], and we have suppressed the fermion spin index for readability. The interaction vertices are obtained from the original $g_{F1,2}$ after Bogoliubov transformation of the bosons, which couples the fermions to the normal modes of the BEC (see Supplement for details).

In the following we assume, for simplicity, equal densities $n_1 = n_2 = n_F = n$ and equal masses $m_1 = m_2 = m_F = m$; our results are qualitatively similar for density or mass imbalances systems. Under these assumptions, we find that the effective spin vertex $M_s(q) \simeq \sqrt{2n}g_F\sqrt{(q^2/2m)/\omega_q^s} \sim \sqrt{q/c_s}$ with $g_F \equiv (g_{F1} - g_{F2})/2$ resembles the conventional electron-phonon coupling introduced by Fröhlich [20] [near the transition to the droplet state the soft density normal mode couples to fermions with effective coupling $g_F = (g_{F1} + g_{F2})/2$]. In our case, however, near the spinodal point the spin dispersion in the denominator becomes soft and enhances the interaction vertex towards $M_s(q) \simeq \sqrt{2n}g_F$, while the density vertex $M_d(q) \sim \sqrt{q}$ is suppressed for small q.

In analogy with the electron-phonon problem, the Bose-Fermi interaction in our system induces interactions between fermions. Following the treatment of Ref. [21],
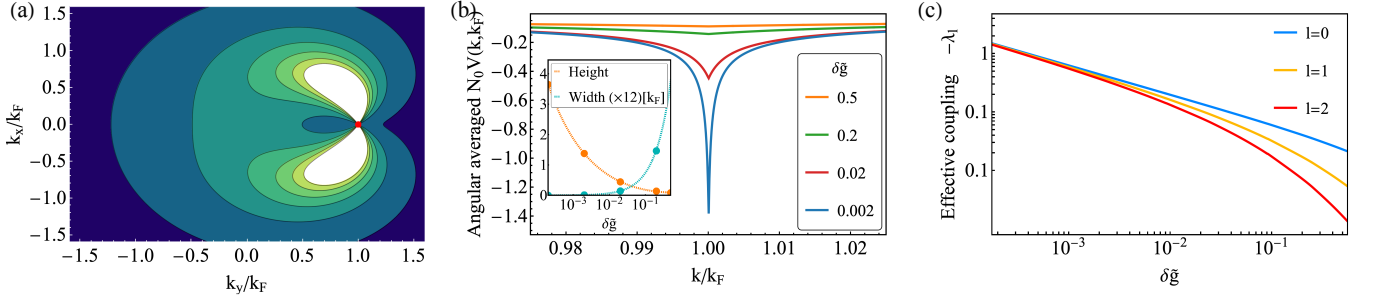
Figure 2. Effective induced electron-electron interaction. (a) Effective electron-electron interaction $V_{\mathbf{kk'}}$ in Eq. (8) as a function of $\mathbf{k} = (k_x, k_y)$ near the spinodal instability with $\delta\tilde{g} \equiv (m/\hbar^2)\delta g = 0.001$ and $\tilde{g}_F \equiv (m/\hbar^2)g_F = 0.2$. The second fermion momentum $\mathbf{k'} = (k_F, 0)$ is placed at the Fermi surface (red dot). The induced interaction is strongly enhanced in forward direction $\mathbf{k} \approx \mathbf{k'}$. (b) Effective azimuthal-averaged interaction $V(k, k' = k_F)$ in the vicinity of the Fermi surface as a function of the radial momentum $k = |\mathbf{k}|$ for different values of $\delta\tilde{g}$, showing the resonant behaviour as $\delta\tilde{g} \searrow 0$. Inset: height and full width at half maximum of the effective interaction peak at the Fermi surface for various values of $\delta\tilde{g}$, characterizing the resonant scaling behaviour as $\delta\tilde{g} \searrow 0$; the dashed lines guide the eye. (c) Effective coupling λ_ℓ [Eq. (9)] in angular momentum channels $\ell = 0$ to $\ell = 2$ as a function of $\delta\tilde{g}$.

we calculate the induced interaction potential between Cooper pairs of fermions $(\mathbf{k}, -\mathbf{k})$ and $(\mathbf{k'}, -\mathbf{k'})$,

$$V_{\mathbf{kk'}} = -\frac{|M_d(\mathbf{q})|^2 \omega_{\mathbf{q}}^d}{(\omega_{\mathbf{q}}^d)^2 + (\epsilon_{\mathbf{k'}} - \epsilon_{\mathbf{k}})^2} - \frac{|M_s(\mathbf{q})|^2 \omega_{\mathbf{q}}^s}{(\omega_{\mathbf{q}}^s)^2 + (\epsilon_{\mathbf{k'}} - \epsilon_{\mathbf{k}})^2}, \quad (7)$$

where $\mathbf{q} = \mathbf{k'} - \mathbf{k}$ is the exchanged momentum between fermion pairs. The $+$ sign in the denominator arises from renormalization that avoids spurious singularities from normal mode emission and absorption [22]. Near the spinodal point, the contribution from the soft spin modes dominates over the contribution from the density modes, and the induced potential takes the Ornstein–Zernike form

$$V_{\mathbf{kk'}} \approx -\frac{2n g_F^2 q^2/2m}{c_s^2 q^2 (1 + q^2 \xi_s^2) + (\epsilon_{\mathbf{k+q}} - \epsilon_{\mathbf{k}})^2} \quad (8)$$

with spin healing length $\xi_s = \hbar/2mc_s = \hbar/\sqrt{4m\,\delta g\,n}$. The full two-dimensional momentum dependence of this induced potential is shown in Fig. 2(a): it is strongly enhanced near the Fermi surface and in the forward direction $\mathbf{k} \approx \mathbf{k'}$ ($q \to 0$).

The enhancement of the induced potential near the Fermi surface is also apparent in the azimuthal average $V(k, k')$ over the angle $\mathbf{k} \cdot \mathbf{k'} = kk' \cos\theta$ at fixed modulus k, k'. For one fermion $k' = k_F$ fixed at the Fermi surface, the dependence on the other fermion momentum k becomes strongly peaked at $k = k_F$ for smaller values of δg, as shown in Fig. 2(b). As we approach the spinodal instability $\delta g \to 0$, the peak depth of the induced potential grows as $(\delta g)^{-1/2}$ while the width of the peak is reduced as $(\delta g)^{1/2}$ (see inset).

For scattering between Cooper pairs at the Fermi surface the fermionic energy exchange in the denominator vanishes, and the induced potential takes the resonance form $V_{\mathbf{kk'}} \approx -(g_F^2/\delta g)/(1 + q^2 \xi_s^2)$. The width of the resonance is given by the inverse spin healing length ξ_s^{-1},

which marks the crossover wave number between linear and quadratic spin-wave dispersion. Near the spinodal point $\delta g \searrow 0$ this becomes much smaller than the standard inverse healing length $\xi^{-1} = \sqrt{2mgn}$ of a single bosonic component. Conversely, the strong induced potential extends to much larger range ξ_s in real space before it crosses over into a van der Waals tail [23].

Since the induced potential at the Fermi surface is strongly peaked in forward direction $\theta \to 0$, a partial wave decomposition of $V_{\mathbf{kk'}}$ yields substantial contributions also for higher angular momentum channels $\ell = 1, 2, \ldots$ [24]. We define the effective dimensionless coupling λ_ℓ in the ℓ partial-wave channel in two dimensions, in analogy with the three-dimensional case [25],

$$\lambda_\ell = N_0 \int_0^{2\pi} \frac{d\theta}{2\pi} \cos(\ell\theta) V_{\mathbf{kk'}}\big|_{|\mathbf{k}|=|\mathbf{k'}|=k_F} \quad (9)$$

with $q^2 = |\mathbf{k} - \mathbf{k'}|^2 = 2k_F^2(1 - \cos\theta)$ for $|\mathbf{k}| = |\mathbf{k'}| = k_F$. The leading couplings for s-wave ($\ell = 0$) and p-wave ($\ell = 1$) pairing are

$$\lambda_0 = -\alpha \frac{4k_F^2 \xi_s^2}{\sqrt{1 + 4k_F^2 \xi_s^2}}, \quad \lambda_1 = -\alpha \frac{(\sqrt{1 + 4k_F^2 \xi_s^2} - 1)^2}{\sqrt{1 + 4k_F^2 \xi_s^2}} \quad (10)$$

with dimensionless coefficient $\alpha = (N_0 g_F^2/\delta g)/(4k_F^2 \xi_s^2) = \frac{1}{4}(N_0 g_F)^2 (mn/m_F n_F)$, where we have reinstated the fermion mass m_F and the fermion density n_F to illustrate the effect of mass or density imbalance. The effective couplings λ_ℓ in different angular momentum channels are shown in Fig. 2(c) as a function of $\delta\tilde{g}$. While far from the spinodal point the s-wave channel ($\ell = 0$) dominates, we observe that the $\ell > 0$ contributions become comparable to the s-wave channel as we approach the spinodal instability. Near the spinodal instability $\xi_s \to \infty$ and the interaction in all channels diverges linearly in ξ_s as $\lambda_\ell \approx -\alpha\, 2k_F\xi_s$, as seen in Fig. 2(c).

Pairing gap and critical temperature. The induced attractive interaction between fermions at the Fermi surface leads to Cooper pairing in analogy with phonon-mediated pairing in conventional BCS superconductors. From the induced interaction potential, we calculate the fermion pairing gap $\Delta(\mathbf{k})$ in our system by solving the BCS gap equation [1, 24, 26]

$$\Delta(\mathbf{k}) = -\sum_{\mathbf{k}'} V_{\mathbf{k}\mathbf{k}'} \frac{\Delta(\mathbf{k}')}{2E(\mathbf{k}')} \tanh\left(\frac{E(\mathbf{k}')}{2k_B T}\right) \qquad (11)$$

with BCS quasiparticle energy $E(\mathbf{k}) = \sqrt{\xi_{\mathbf{k}}^2 + |\Delta(\mathbf{k})|^2}$ and fermion energy $\xi_{\mathbf{k}} = \epsilon_{\mathbf{k}} - \mu_F$ measured from the fermion chemical potential. At weak coupling only fermions near the Fermi surface contribute to pairing, and the radial $|\mathbf{k}'|$ integral decouples from the integration over the scattering angle θ between Cooper pairs at $\mathbf{k}$ and $\mathbf{k}'$. One can then directly use the effective couplings λ_ℓ from Eq. (9) to obtain the gap $\Delta_\ell \propto \exp(1/\lambda_\ell)$ at zero temperature [24]. At larger coupling the radial and azimuthal integrals no longer decouple and we find the gap by numerical integration.

In Fig. 3 we characterize the superconducting, paired state, by solving the gap equation for different values of the inter-species interactions and for different symmetries of the gap parameter. First, Fig. 3(a) shows the s-wave gap Δ, calculated at the Fermi surface as a function of the temperature, for different values of the detuning $\delta\tilde{g}$. It clearly shows that pairing is enhanced as the spinodal instability $\delta\tilde{g} \searrow 0$ is approached and the spin normal mode becomes soft. Second, Fig. 3(b) displays the pairing gap in different angular momentum channels $\ell = 0, 1, 2$. It shows that also higher angular momentum channels $\ell > 0$ have sizeable gaps, while the strongest pairing still occurs in the s-wave channel ($\ell = 0$). Finally, Fig. 3(c) exhibits the critical temperature T_c in different angular momentum channels. We find that T_c, as found from the numerical solution of the gap equation, is significantly enhanced to reach several percent of the Fermi temperature as the resonant regime is approached.

Experimental realizations. We now discuss two realistic scenarios where the present theoretical prediction could be experimentally observed: (a) A two-component gas of excitons or exciton-polaritons coexisting with a two-spin Fermi gas of electrons in 2D semiconductors, and (b) ultracold atomic Bose-Fermi mixtures.

Exciton-electron systems in 2D semiconductors. The basic requirement in order to realize spinor-BEC mediated superconductivity is a two-component bosonic system with tunable interactions coupled to a fermionic system. This condition is fulfilled in solid-state van der Waals heterostructures consisting of monolayer transition dichalcogenide (TMD) semiconductors such as Molybdenum diselenide (MoSe$_2$). The elementary bosonic excitations in these systems are excitons, which are optically excited electron-hole bound pairs. The ultrastrong exciton binding energy of about $200\,\mathrm{meV}$ in these TMD monolayers means that the excitons are robust and can be considered as point-like bosons at cryogenic temperatures $T \sim 4\,\mathrm{K}$ [27]. Moreover, the valley degree of freedom in TMD monolayers allows to selectively address two components (1 and 2) of excitons using circularly polarized illumination. In addition, itinerant charges (electrons or holes) can be introduced in the system through electrical contacts, and their densities can be tuned using proximal gate electrodes. At exciton densities lower than the Mott density $n_X \gtrsim 10^{13}\,\mathrm{cm}^{-2}$, the interactions between excitons are short-ranged and can be approximated as contact-like. In general, interactions between excitons of the same valley are repulsive with typical values of $g_{11} \simeq g_{22} \simeq 0.1\,\mu\mathrm{eV}\mu\mathrm{m}^2$ [28, 29], whereas the inter-valley exciton interactions $g_{12} < 0$ are attractive, leading to a molecular biexciton bound state with binding energy $E_{BX} \simeq 20\,\mathrm{meV}$.

For tuning the inter-valley exciton interactions, we refer to several possible schemes that have been previously proposed or demonstrated [30–32]. In bare monolayer heterostructures (i.e. not coupled to cavities), a Feshbach-like scenario has been shown, where the molecular biexciton state between opposite valley excitons is brought into resonance with the free exciton state by means of a two-photon process, in analogy with optical Feshbach resonances in ultracold atomic systems [31–33]. In this case, by detuning an optical dressing field around the biexciton resonance, the effective inter-valley exciton-exciton interaction strength may be tuned from strongly attractive to repulsive. A similar scheme has also been shown in III-V semiconductors heterostructures coupled to optical cavities, where the hybridization between excitons and cavity photons leads to new quasiparticles known as exciton-polaritons. A biexcitonic Feshbach resonance effect with exciton-polaritons was demonstrated by tuning the lower exciton-polariton branch into resonance with the biexciton state [30]. Another intriguing possibility is to use long-lived inter-layer exciton condensates, where the electron and hole are spatially separated in two layers giving them a permanent electric dipole moment. A Feshbach resonance between such inter-layer excitons has been proposed in [34] using dc electric fields to tune the states into resonance. In all these cases, the main idea is to reach the instability in the two-component Bose gas by tuning the inter-valley scattering either to the spinodal point for repulsive $g_{12} = g = g_{11} = g_{22}$ or to the onset of the droplet state for attractive $g_{12} = -g$.

An important feature of TMD heterostructures is the ability to inject itinerant electrons (or holes) in the semiconductor through electrical contacts, and tune their density using proximal gate electrodes - while maintaining a coexisting population of excitons. The interaction between excitons and electrons is strong and attractive between particles of different valleys, leading to an inter-valley molecular Trion-bound state with bind-
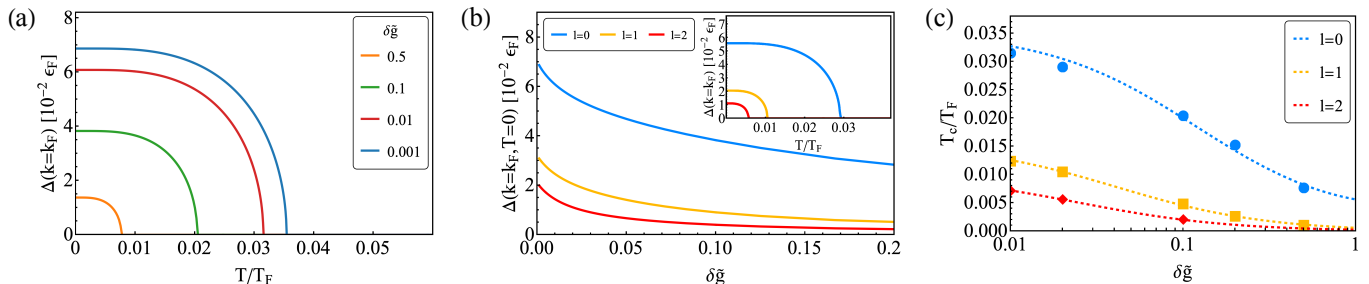
Figure 3. **Fermion-fermion pairing and superconductivity.** (a) Zero-temperature s-wave pairing gap Δ as a function of temperature T/T_F for different values of detuning $\delta\tilde{g} \equiv (m/\hbar^2)\delta g$, with $\tilde{g}_F \equiv (m/\hbar^2)g_F = 2.0$. (b) Zero-temperature pairing gap Δ_ℓ vs. detuning $\delta\tilde{g}$ for different angular momentum channels: all pairing gaps are enhanced for small $\delta\tilde{g}$ near the spinodal point. Inset: pairing gap Δ_ℓ vs. temperature T/T_F for fixed $\delta\tilde{g} = 0.02$. (c) Critical temperature T_c vs. detuning $\delta\tilde{g}$; near the spinodal point T_c reaches large values even in higher angular momentum channels because of the resonant induced interaction. The dashed lines guide the eye.

ing energy $E_T \sim 25$ meV [27, 35]. Electron densities of up to $n_e \sim 1 \times 10^{12}$ cm^{-2} can be routinely obtained by tuning the gate electrode potential. Using sufficiently intense resonant illumination, the exciton density can be tuned to reach the same order of magnitude, resulting in a Bose–Fermi mixture with tunable densities and exciton-exciton interactions [28]. Using the following parameters for TMD heterostructures: effective electron mass $m^* = 0.7m_e$ and $n_e \sim 1 \times 10^{12}$ cm^{-2}, we obtain a Fermi energy $\epsilon_F = \frac{\pi\hbar^2}{m^*}n_e = 3.4$ meV corresponding to a Fermi temperature $T_F = \epsilon_F/k_B \approx 40$ K. Following the results in Fig.3a, for $\delta\tilde{g} = 10^{-3}$, we estimate the s-wave zero-temperature pairing gap of $\Delta \approx 0.07 \times \epsilon_F \approx 0.24$ meV and critical superconducting temperature of $T_c \approx 1.3$ K. These quantities can be experimentally measured in standard cryostats using well established 4-point dc transport experiments or more advanced ultrafast ac conductivity experiments using THz waveguides in case pulsed laser excitation is used to create the exciton gas [36].

Ultracold atomic Bose–Fermi mixtures. Mixtures of bosonic and fermionic atoms at ultracold temperatures have been experimentally realized by a number of groups [37–40]. One realization builds on a homonuclear ^{39}K-^{39}K Bose-Bose mixture [41] where the condensate atoms are in the $(F = 1, m_F = -1)$ and $(F = 1, m_F = 0)$ hyperfine states.

For this proposal, we consider using a heteronuclear ^{41}K-^{87}Rb Bose-Bose mixture [19, 42], the atoms in the condensate being in the hyperfine ground state $(F = 1, m_F = 1)$. An easily-accessible Feshbach resonance at $B = 78.9$ G [43–47] allows to tune the inter-component scattering length $a_{\text{K-Rb}}$, whereas the intra-component scattering lengths are approximately constant at $a_{\text{K-K}} \simeq 62\,a_0$ and $a_{\text{Rb-Rb}} \simeq 100.4\,a_0$ in a very wide region around the Feshbach resonance. We also stress that this choice is not affected by spin-changing collisions, which could limit the lifetime of the mixture. On top of this binary mixture, we consider a generic fermionic component—one could

think of different hyperfine states of ^{40}K—interacting with the bosonic components via short-range potentials with scattering lengths $a_{\text{f-Rb}} \simeq a_{\text{f-K}} \simeq 50\,a_0$, noting that this choice of parameters does not affect the qualitative behaviour of the physical mechanism we aim to investigate. Different schemes could be employed to observe the onset of pairing and superfluidity in the fermionic system, for example using spatially resolved quasiparticle spectroscopy [48, 49], measurement of the momentum distribution using matterwave optics [50] or Bragg spectroscopy [51, 52].

Discussion. We show that fine-tuning the interactions of a bosonic medium allows for substantial enhancement of the induced interactions between fermions. Our proposed method is intrinsically different from Feshbach resonances, since we achieve resonant interactions while keeping finite scattering lengths within and between the two species. The controlled softening of the spin-wave mode close to the spinodal point is achieved while maintaining phase-stiffness of the BEC, which leads to robust collective excitations. Therefore, our method is fundamentally different from the vanishing sound velocity of a noninteracting BEC, which becomes unstable in the presence of fermions [53].

Thus, the present system represents a novel form of strongly correlated quantum matter, where the conventional BCS phenomenology can be tested to its limits in a real solid-state device. It is worth noting that the experimental parameters in our proposals will allow to reach a critical temperature $T_c/T_F \approx 0.03$, which is within the range of applicability of BCS theory. At smaller values of δg the induced interaction will grow beyond the BCS regime, realizing a solid-state equivalent of the celebrated BEC-BCS crossover [3]. We note that the BCS approximation has proved reliable in predicting the pairing energy of real fermions throughout the crossover [49].

The similarity between the present picture and the physics of ultracold fermionic atoms runs even deeper

than their BCS description. In both cases, the appearance of strong correlation physics at finite temperature is the consequence of an underlying zero-temperature quantum critical point [54]. In the present scenario, the quantum critical point separates the homogeneous BEC from either a phase separated or a droplet state at $\delta g < 0$ [17, 18, 55]. Thanks to the softening of normal mode excitations at criticality the effective interaction mediated by the spinor BEC grows substantially, see Fig. 2(b), increases the pairing in all channels, see Figs. 3(a) and (b), and causes the enhancement of critical temperatures observed in Fig. 3(c).

In conclusion, our predictions describe a novel way to tailor interactions between Fermi particles that is different from the traditional picture of the Feshbach resonance, where one tailors the two-body properties in vacuum in order to achieve strong many-body correlations. Here, we exploit the presence of a coherent medium, the spinor

BEC, whose properties can be altered in order to control the interaction in a target system, the fermions, see Fig. 1. Our framework applies generically and hence can be used to achieve strong correlations both in condensed matter and AMO systems as we argue in the section on *Experimental realizations*. We envisage that the present mechanism could serve to realize a light-induced BCS state whose critical temperature rises well above current limits [56–58].

Supplement: Resonantly enhanced superconductivity mediated by spinor condensates

Normal modes of the spinor BEC

Let us start from the real-space Hamiltonian of a two-component, two-dimensional Bose gas, with two spin components labeled 1 and 2,

$$\hat{H} = \int \mathrm{d}^2 r \left(\sum_{i=1,2} \psi_i^\dagger(\mathbf{r}) \left(-\frac{\hbar^2}{2m_i}\nabla^2 + \frac{g_{ii}}{2}|\psi_i(\mathbf{r})|^2 \right) \psi_i(\mathbf{r}) + g_{12}|\psi_1(\mathbf{r})|^2|\psi_2(\mathbf{r})|^2 \right), \tag{12}$$

where the $\psi_i^\dagger(\mathbf{r})$ ($\psi_i(\mathbf{r})$) field operator creates (annihilates) bosons of species i at position $\mathbf{r}$, respectively, and m_i is the boson mass for species i. Moreover, as in the main text, g_{11} and g_{22} are the coupling constants between bosons of species 1 and 2, respectively, and g_{12} is the coupling strength between species 1 and 2.

One can then expand the field operators

$$\hat{\psi}_1(\mathbf{r}) = \frac{1}{\sqrt{V}} \sum_{\mathbf{q}} e^{i\mathbf{q}\cdot\mathbf{r}} \hat{\alpha}_{\mathbf{q}}, \tag{13}$$

$$\hat{\psi}_2(\mathbf{r}) = \frac{1}{\sqrt{V}} \sum_{\mathbf{q}} e^{i\mathbf{q}\cdot\mathbf{r}} \hat{\beta}_{\mathbf{q}}, \tag{14}$$

in bosonic field operators $\hat{\alpha}_{\mathbf{q}}$ and $\hat{\beta}_{\mathbf{q}}$ in Fourier space. In the low-energy limit one can follow the Bogoliubov approach [59] and separate the macroscopic occupation of the lowest-energy mode from the fluctuations at $\mathbf{k} \neq 0$,

$$\hat{\alpha}_{\mathbf{k}} = (2\pi)^2 \sqrt{n_1} \delta(\mathbf{k}) + \hat{A}_{\mathbf{k}\neq 0}, \tag{15}$$

$$\hat{\beta}_{\mathbf{k}} = (2\pi)^2 \sqrt{n_2} \delta(\mathbf{k}) + \hat{B}_{\mathbf{k}\neq 0}. \tag{16}$$

In the following we retain only quadratic terms in $\hat{A}_{\mathbf{k}}$ and $\hat{B}_{\mathbf{k}}$ and neglect higher-order terms. Finally, the Bogoliubov transformation brings the quadratic Hamiltonian into a diagonal form. For the spinor BEC the Bogoliubov transformation is given by a 4×4 matrix that rotates the creation and annihilation operators for the two species into density and spin normal modes [60],

$$\begin{pmatrix} \hat{A}_{\mathbf{k}} \\ \hat{A}_{-\mathbf{k}}^\dagger \\ \hat{B}_{\mathbf{k}} \\ \hat{B}_{-\mathbf{k}}^\dagger \end{pmatrix} = \begin{pmatrix} M_{\mathbf{k}}^{11} & M_{\mathbf{k}}^{12} & M_{\mathbf{k}}^{13} & M_{\mathbf{k}}^{14} \\ M_{\mathbf{k}}^{21} & M_{\mathbf{k}}^{22} & M_{\mathbf{k}}^{23} & M_{\mathbf{k}}^{24} \\ M_{\mathbf{k}}^{31} & M_{\mathbf{k}}^{32} & M_{\mathbf{k}}^{33} & M_{\mathbf{k}}^{34} \\ M_{\mathbf{k}}^{41} & M_{\mathbf{k}}^{42} & M_{\mathbf{k}}^{43} & M_{\mathbf{k}}^{44} \end{pmatrix} \begin{pmatrix} \hat{a}_{\mathbf{k}} \\ \hat{a}_{-\mathbf{k}}^\dagger \\ \hat{b}_{\mathbf{k}} \\ \hat{b}_{-\mathbf{k}}^\dagger \end{pmatrix}. \tag{17}$$

The matrix elements $M_{\mathbf{k}}^{ij}$ are derived and given explicitly in Ref. [60]. In the basis of density normal modes $\hat{a}_{\mathbf{k}}$, $\hat{a}_{\mathbf{k}}^{\dagger}$ and spin normal modes $\hat{b}_{\mathbf{k}}$, $\hat{b}_{\mathbf{k}}^{\dagger}$ one arrives at the spinor-BEC Hamiltonian that we report in the main text,

$$\hat{H} = \sum_{\mathbf{k}} \omega_{\mathbf{k}}^{d} \hat{a}_{\mathbf{k}}^{\dagger} \hat{a}_{\mathbf{k}} + \sum_{\mathbf{k}} \omega_{\mathbf{k}}^{s} \hat{b}_{\mathbf{k}}^{\dagger} \hat{b}_{\mathbf{k}}. \tag{18}$$

The normal mode dispersion relations for the density and spin modes, $\omega_{\mathbf{k}}^{d}$ and $\omega_{\mathbf{k}}^{s}$, are given explicitly in Ref. [60].

Derivation of the interaction vertex

Let us now introduce a fermion interacting with the two original bosonic species 1 and 2,

$$\hat{H}_{\text{f-bos}} = g_{F1} \sum_{\mathbf{k},\mathbf{q}} \hat{\rho}(\mathbf{q}) \hat{\alpha}_{\mathbf{k}-\mathbf{q}}^{\dagger} \hat{\alpha}_{\mathbf{k}} + g_{F2} \sum_{\mathbf{k},\mathbf{q}} \hat{\rho}(\mathbf{q}) \hat{\beta}_{\mathbf{k}-\mathbf{q}}^{\dagger} \hat{\beta}_{\mathbf{k}}, \tag{19}$$

where g_{Fi} is the coupling constant between the fermion and the bosons in the i component and $\hat{\rho}(\mathbf{q}) = \exp(i\mathbf{q} \cdot \hat{\mathbf{R}})$ is the Fourier transform of the density of a single, first-quantized fermion located at position $\hat{\mathbf{R}}$. Again, we can make use of Bogoliubov approximation as in Eqs. (15, 16) and rewrite Eq. (19) as

$$\hat{H}_{\text{f-bos}} = g_{F1}\sqrt{n_1} \sum_{\mathbf{k}\neq 0} e^{i\mathbf{k}\cdot\hat{\mathbf{R}}}(\hat{A}_{\mathbf{k}} + \hat{A}_{-\mathbf{k}}^{\dagger}) + g_{F2}\sqrt{n_2} \sum_{\mathbf{k}\neq 0} e^{i\mathbf{k}\cdot\hat{\mathbf{R}}}(\hat{B}_{\mathbf{k}} + \hat{B}_{-\mathbf{k}}^{\dagger}) \tag{20}$$

to leading order in $\hat{A}_{\mathbf{k}}$ and $\hat{B}_{\mathbf{k}}$ — the so-called Fröhlich approximation [61]. We having omitted a constant energy offset. The Bogoliubov transformation in Eq. (17) then gives

$$\hat{H}_{\text{f-bos}} = g_{F1}\sqrt{n_1} \sum_{\mathbf{k}\neq 0} e^{i\mathbf{k}\cdot\hat{\mathbf{R}}}[(M_{\mathbf{k}}^{11} + M_{\mathbf{k}}^{21})\hat{a}_{\mathbf{k}} + (M_{\mathbf{k}}^{12} + M_{\mathbf{k}}^{22})\hat{a}_{-\mathbf{k}}^{\dagger}] \tag{21}$$

$$+ g_{F1}\sqrt{n_1} \sum_{\mathbf{k}\neq 0} e^{i\mathbf{k}\cdot\hat{\mathbf{R}}}[(M_{\mathbf{k}}^{13} + M_{\mathbf{k}}^{23})\hat{b}_{\mathbf{k}} + (M_{\mathbf{k}}^{14} + M_{\mathbf{k}}^{24})\hat{b}_{-\mathbf{k}}^{\dagger}] \tag{22}$$

$$+ g_{F2}\sqrt{n_2} \sum_{\mathbf{k}\neq 0} e^{i\mathbf{k}\cdot\hat{\mathbf{R}}}[(M_{\mathbf{k}}^{31} + M_{\mathbf{k}}^{41})\hat{a}_{\mathbf{k}} + (M_{\mathbf{k}}^{32} + M_{\mathbf{k}}^{42})\hat{a}_{-\mathbf{k}}^{\dagger}] \tag{23}$$

$$+ g_{F2}\sqrt{n_2} \sum_{\mathbf{k}\neq 0} e^{i\mathbf{k}\cdot\hat{\mathbf{R}}}[(M_{\mathbf{k}}^{33} + M_{\mathbf{k}}^{43})\hat{b}_{\mathbf{k}} + (M_{\mathbf{k}}^{34} + M_{\mathbf{k}}^{44})\hat{b}_{-\mathbf{k}}^{\dagger}]. \tag{24}$$

One can rewrite the interaction term for coupling the fermion to both density and spin normal modes as

$$\hat{H}_{\text{f-bos}} = \sum_{\mathbf{k}\neq 0} M_d(\mathbf{k}) e^{i\mathbf{k}\cdot\hat{\mathbf{R}}}(\hat{a}_{\mathbf{k}} + \hat{a}_{-\mathbf{k}}^{\dagger}) + \sum_{\mathbf{k}\neq 0} M_s(\mathbf{k}) e^{i\mathbf{k}\cdot\hat{\mathbf{R}}}(\hat{b}_{\mathbf{k}} + \hat{b}_{-\mathbf{k}}^{\dagger}). \tag{25}$$

Here, we have introduced the density and spin interaction matrix elements

$$M_d(\mathbf{k}) = g_{F1}\sqrt{n_1}(M_{\mathbf{k}}^{11} + M_{\mathbf{k}}^{21}) + g_{F2}\sqrt{n_2}(M_{\mathbf{k}}^{31} + M_{\mathbf{k}}^{41}) \, , \tag{26}$$

$$M_s(\mathbf{k}) = g_{F1}\sqrt{n_1}(M_{\mathbf{k}}^{13} + M_{\mathbf{k}}^{23}) + g_{F2}\sqrt{n_2}(M_{\mathbf{k}}^{33} + M_{\mathbf{k}}^{43}) \tag{27}$$

using symmetric $M_{\mathbf{k}}^{11} + M_{\mathbf{k}}^{21} = M_{\mathbf{k}}^{12} + M_{\mathbf{k}}^{22}$ and analogously for the 3, 4 components. As a consistency check one confirms [60] that when the interactions between different bosonic species are turned off, assuming the same boson-boson scattering length for both species, the matrix in Eq. (17) becomes block diagonal as

$$\begin{pmatrix} \hat{A}_{\mathbf{k}} \\ \hat{A}_{-\mathbf{k}}^{\dagger} \\ \hat{B}_{\mathbf{k}} \\ \hat{B}_{-\mathbf{k}}^{\dagger} \end{pmatrix} = \begin{pmatrix} u_{\mathbf{k}} & v_{-\mathbf{k}}^{*} & 0 & 0 \\ v_{\mathbf{k}} & u_{-\mathbf{k}}^{*} & 0 & 0 \\ 0 & 0 & u_{\mathbf{k}} & v_{-\mathbf{k}}^{*} \\ 0 & 0 & v_{\mathbf{k}} & u_{-\mathbf{k}}^{*} \end{pmatrix} \begin{pmatrix} \hat{a}_{\mathbf{k}} \\ \hat{a}_{-\mathbf{k}}^{\dagger} \\ \hat{b}_{\mathbf{k}} \\ \hat{b}_{-\mathbf{k}}^{\dagger} \end{pmatrix} \tag{28}$$

with the Bogoliubov coherence factors $u_{\mathbf{k}}$, $v_{\mathbf{k}}$ [62]. In this case one readily recovers the standard interaction matrix elements [61] with $\omega_{\mathbf{k}}^{(0)} = k^2/2m$,

$$M_d(\mathbf{k}) = g_{F1}\sqrt{n_1}\sqrt{\frac{\omega_{\mathbf{k}}^{(0)}}{\omega_{\mathbf{k}}}}, \qquad\qquad M_s(\mathbf{k}) = g_{F2}\sqrt{n_2}\sqrt{\frac{\omega_{\mathbf{k}}^{(0)}}{\omega_{\mathbf{k}}}} \tag{29}$$

using the identity $u_\mathbf{k} + v_\mathbf{k} = \sqrt{\omega_\mathbf{k}^{(0)}/\omega_\mathbf{k}}$.

In general for the interacting spinor BEC, the interaction vertex between the fermion and the normal modes can be written as (assuming symmetric $n_1 = n_2 = n$, $m_1 = m_2 = m$ and $g_{11} = g_{22} = g$)

$$M_d(\mathbf{k}) = \sqrt{2n}\,\frac{g_{F1} + g_{F2}}{2}\left[\sqrt{\frac{\omega_\mathbf{k}^{(0)} + (g + g_{12})n + \omega_\mathbf{k}^d}{2\omega_\mathbf{k}^d}} - \sqrt{\frac{\omega_\mathbf{k}^{(0)} + (g + g_{12})n - \omega_\mathbf{k}^d}{2\omega_\mathbf{k}^d}}\right],$$

$$M_s(\mathbf{k}) = \sqrt{2n}\,\frac{g_{F1} - g_{F2}}{2}\left[\sqrt{\frac{\omega_\mathbf{k}^{(0)} + (g - g_{12})n + \omega_\mathbf{k}^s}{2\omega_\mathbf{k}^s}} - \sqrt{\frac{\omega_\mathbf{k}^{(0)} + (g - g_{12})n - \omega_\mathbf{k}^s}{2\omega_\mathbf{k}^s}}\right].$$

We define the effective fermion-spin coupling $g_F = (g_{F1} - g_{F2})/2$ and expand the spin-fermion vertex for small $\delta g = g - g_{12}$ near the transition to phase separation as

$$M_s(\mathbf{k}) = \sqrt{2n}\,g_F\left(1 - \frac{\delta g\, n}{2\omega_\mathbf{k}^{(0)}} + \mathcal{O}(\delta g^2)\right). \tag{30}$$

For small δg this is well approximated by the leading constant term. At the same time, the density-fermion vertex remains suppressed. Near the transition to the droplet phase, instead, the density normal modes become soft and the density-fermion vertex is enhanced, while the spin-fermion vertex remains suppressed for small momenta.

[1] J. Bardeen, L. N. Cooper, and J. R. Schrieffer, Phys. Rev. **108**, 1175 (1957).

[2] Y. Cao, V. Fatemi, S. Fang, K. Watanabe, T. Taniguchi, E. Kaxiras, and P. Jarillo-Herrero, Nature **556**, 43 (2018).

[3] W. Zwerger, ed., *The BCS-BEC Crossover and the Unitary Fermi Gas*, Lecture Notes in Physics, Vol. 836 (Springer, Berlin, 2011).

[4] O. Cotlet, S. Zeytinoglu, M. Sigrist, E. Demler, and A. Imamoglu, Phys. Rev. B **93**, 054510 (2016).

[5] D. Suchet, Z. Wu, F. Chevy, and G. M. Bruun, Phys. Rev. A **95**, 043643 (2017).

[6] A. Camacho-Guardian, M. Bastarrachea-Magnani, and G. Bruun, Phys. Rev. Lett. **126**, 017401 (2021).

[7] M. A. Bastarrachea-Magnani, A. Camacho-Guardian, and G. M. Bruun, Phys. Rev. Lett. **126**, 127405 (2021).

[8] D. Fausti, R. I. Tobey, N. Dean, S. Kaiser, A. Dienst, M. C. Hoffmann, S. Pyon, T. Takayama, H. Takagi, and A. Cavalleri, Science **331**, 189 (2011).

[9] M. Mitrano, A. Cantaluppi, D. Nicoletti, S. Kaiser, A. Perucchi, S. Lupi, P. Di Pietro, D. Pontiroli, M. Riccò, S. R. Clark, D. Jaksch, and A. Cavalleri, Nature **530**, 461 (2016).

[10] B. Liu, M. Först, M. Fechner, D. Nicoletti, J. Porras, T. Loew, B. Keimer, and A. Cavalleri, Phys. Rev. X **10**, 011053 (2020).

[11] L. P. Pitaevskii and S. Stringari, *Bose-Einstein Condensation* (Clarendon Press, Oxford, 2003).

[12] D. M. Larsen, Annals of Physics **24**, 89 (1963).

[13] Y. Kawaguchi and M. Ueda, Physics Reports **520**, 253 (2012).

[14] D. M. Stamper-Kurn and M. Ueda, Rev. Mod. Phys. **85**, 1191 (2013).

[15] V. Karle, N. Defenu, and T. Enss, Phys. Rev. A **99**, 063627 (2019).

[16] A. Recati and S. Stringari, Annu. Rev. Condens. Matter Phys. **13**, 407 (2022).

[17] D. S. Petrov, Phys. Rev. Lett. **115**, 155302 (2015).

[18] D. S. Petrov and G. E. Astrakharchik, Phys. Rev. Lett. **117**, 100401 (2016).

[19] G. Bighin, A. Burchianti, F. Minardi, and T. Macrì, Phys. Rev. A **106**, 023301 (2022).

[20] H. Fröhlich, Advances in Physics **3**, 325 (1954).

[21] T. Enss and W. Zwerger, Eur. Phys. J. B **68**, 383 (2009).

[22] P. Lenz and F. Wegner, Nucl. Phys. B **482**, 693 (1996).

[23] K. Fujii, M. Hongo, and T. Enss, Phys. Rev. Lett. **129**, 233401 (2022).

[24] P. W. Anderson and P. Morel, Phys. Rev. **123**, 1911 (1961).

[25] H. Heiselberg, C. J. Pethick, H. Smith, and L. Viverit, Phys. Rev. Lett. **85**, 2418 (2000).

[26] A. J. Leggett, *Quantum Liquids: Bose condensation and Cooper pairing in condensed-matter systems* (Oxford University Press, Oxford, 2008).

[27] G. Wang, A. Chernikov, M. M. Glazov, T. F. Heinz, X. Marie, T. Amand, and B. Urbaszek, Rev. Mod. Phys. **90**, 021001 (2018).

[28] L. B. Tan, O. Cotlet, A. Bergschneider, R. Schmidt, P. Back, Y. Shimazaki, M. Kroner, and A. Imamoğlu, Phys. Rev. X **10**, 021011 (2020).

[29] G. Li, M. M. Parish, and J. Levinsen, Phys. Rev. B **104**, 245404 (2021).

[30] N. Takemura, S. Trebaol, M. Wouters, M. T. Portella-Oberli, and B. Deveaud, Nature Phys. **10**, 500 (2014).

[31] E. J. Sie, J. W. McIver, Y.-H. Lee, L. Fu, J. Kong, and N. Gedik, Nature Mater. **14**, 290 (2015).

[32] C.-K. Yong, J. Horng, Y. Shen, H. Cai, A. Wang, C.-S. Yang, C.-K. Lin, S. Zhao, K. Watanabe, T. Taniguchi, S. Tongay, and F. Wang, Nature Phys. **14**, 1092 (2018).

[33] C. Chin, R. Grimm, P. Julienne, and E. Tiesinga, Rev. Mod. Phys. **82**, 1225 (2010).

[34] S. V. Andreev, Phys. Rev. B **94**, 140501 (2016).

[35] G. Li, O. Bleu, J. Levinsen, and M. M. Parish, Phys. Rev. B **103**, 195307 (2021).

[36] P. Gallagher, C.-S. Yang, T. Lyu, F. Tian, R. Kou, H. Zhang, K. Watanabe, T. Taniguchi, and F. Wang, Science **364**, 158 (2019), https://www.science.org/doi/pdf/10.1126/science.aat8687.

[37] F. Schreck, L. Khaykovich, K. L. Corwin, G. Ferrari,

T. Bourdel, J. Cubizolles, and C. Salomon, Phys. Rev. Lett. **87**, 080403 (2001).

[38] A. G. Truscott, K. E. Strecker, W. I. McAlexander, G. B. Partridge, and R. G. Hulet, Science **291**, 2570 (2001).

[39] I. Ferrier-Barbut, M. Delehaye, S. Laurent, A. T. Grier, M. Pierce, B. S. Rem, F. Chevy, and C. Salomon, Science **345**, 1035 (2014).

[40] B. J. DeSalvo, K. Patel, G. Cai, and C. Chin, Nature **568**, 61 (2019).

[41] C. R. Cabrera, L. Tanzi, J. Sanz, B. Naylor, P. Thomas, P. Cheiney, and L. Tarruell, Science **359**, 301 (2018).

[42] C. D'Errico, A. Burchianti, M. Prevedelli, L. Salasnich, F. Ancilotto, M. Modugno, F. Minardi, and C. Fort, Phys. Rev. Res. **1**, 033155 (2019).

[43] F. Ferlaino, C. D'Errico, G. Roati, M. Zaccanti, M. Inguscio, G. Modugno, and A. Simoni, Phys. Rev. A **73**, 040702 (2006).

[44] C. D'Errico, M. Zaccanti, M. Fattori, G. Roati, M. Inguscio, G. Modugno, and A. Simoni, New J. Phys. **9**, 223 (2007).

[45] A. Simoni, M. Zaccanti, C. D'Errico, M. Fattori, G. Roati, M. Inguscio, and G. Modugno, Phys. Rev. A **77**, 052705 (2008).

[46] G. Thalhammer, G. Barontini, L. De Sarlo, J. Catani, F. Minardi, and M. Inguscio, Phys. Rev. Lett. **100**, 210402 (2008).

[47] G. Thalhammer, G. Barontini, J. Catani, F. Rabatti, C. Weber, A. Simoni, F. Minardi, and M. Inguscio, New J. Phys. **11**, 055044 (2009).

[48] A. Schirotzek, Y.-i. Shin, C. H. Schunck, and W. Ketterle, Phys. Rev. Lett. **101**, 140403 (2008).

[49] P. A. Murthy, M. Neidig, R. Klemt, L. Bayha, I. Boettcher, T. Enss, M. Holten, G. Zürn, P. M. Preiss, and S. Jochim, Science **359**, 452 (2018).

[50] P. A. Murthy, D. Kedar, T. Lompe, M. Neidig, M. G. Ries, A. N. Wenz, G. Zürn, and S. Jochim, Phys. Rev. A **90**, 043611 (2014).

[51] S. Hoinka, P. Dyke, M. G. Lingham, J. J. Kinnunen, G. M. Bruun, and C. J. Vale, Nature Phys. **13**, 943 (2017).

[52] H. Biss, L. Sobirey, N. Luick, M. Bohlen, J. J. Kinnunen, G. M. Bruun, T. Lompe, and H. Moritz, Phys. Rev. Lett. **128**, 100401 (2022).

[53] S. Ospelkaus, C. Ospelkaus, L. Humbert, K. Sengstock, and K. Bongs, Phys. Rev. Lett. **97**, 120403 (2006).

[54] S. Sachdev, *Quantum Phase Transitions* (Cambridge University Press, Cambridge, 2011).

[55] G. Semeghini, G. Ferioli, L. Masi, C. Mazzinghi, L. Wolswijk, F. Minardi, M. Modugno, G. Modugno, M. Inguscio, and M. Fattori, Phys. Rev. Lett. **120**, 235301 (2018).

[56] K. Katsumi, N. Tsuji, Y. I. Hamada, R. Matsunaga, J. Schneeloch, R. D. Zhong, G. D. Gu, H. Aoki, Y. Gallais, and R. Shimano, Phys. Rev. Lett. **120**, 117001 (2018).

[57] R. Shimano and N. Tsuji, Annu. Rev. Condens. Matter Phys. **11**, 103 (2020).

[58] K. Isoyama, N. Yoshikawa, K. Katsumi, J. Wong, N. Shikama, Y. Sakishita, F. Nabeshima, A. Maeda, and R. Shimano, Commun. Phys. **4**, 160 (2021).

[59] N. N. Bogolyubov, J. Phys. (USSR) **11**, 23 (1947).

[60] D. M. Larsen, Annals of Physics (New York) (U.S.) 10.1016/0003-4916(63)90066-6.

[61] H. Froehlich, Advances in Physics **3**, 325 (1954), https://doi.org/10.1080/00018735400101213.

[62] A. Fetter and J. Walecka, *Quantum Theory of Many-Particle Systems*, Dover Books on Physics (Dover Publications, 2012).